Mitochondrial retrograde signaling regulates neuronal function

Umut Cagin[a,1,2], Olivia F. Duncan[a,1], Ariana P. Gatt[a,1], Marc S. Dionne[b], Sean T. Sweeney[c], and Joseph M. Bateman[a,3]

[a]Wolfson Centre for Age-Related Diseases, Guy's Campus, King's College London, London SE1 1UL, United Kingdom; [b]Department of Life Sciences, South Kensington Campus, Imperial College London, London SW7 2AZ, United Kingdom; and [c]Department of Biology, University of York, Heslington York YO10 5DD, United Kingdom

Edited by Gregory A. Petsko, Weill Cornell Medical College, New York, NY, and approved September 22, 2015 (received for review March 13, 2015)

Mitochondria are key regulators of cellular homeostasis, and mitochondrial dysfunction is strongly linked to neurodegenerative diseases, including Alzheimer's and Parkinson's. Mitochondria communicate their bioenergetic status to the cell via mitochondrial retrograde signaling. To investigate the role of mitochondrial retrograde signaling in neurons, we induced mitochondrial dysfunction in the *Drosophila* nervous system. Neuronal mitochondrial dysfunction causes reduced viability, defects in neuronal function, decreased redox potential, and reduced numbers of presynaptic mitochondria and active zones. We find that neuronal mitochondrial dysfunction stimulates a retrograde signaling response that controls the expression of several hundred nuclear genes. We show that the *Drosophila* hypoxia inducible factor alpha (HIFα) ortholog Similar (Sima) regulates the expression of several of these retrograde genes, suggesting that Sima mediates mitochondrial retrograde signaling. Remarkably, knockdown of Sima restores neuronal function without affecting the primary mitochondrial defect, demonstrating that mitochondrial retrograde signaling is partly responsible for neuronal dysfunction. Sima knockdown also restores function in a *Drosophila* model of the mitochondrial disease Leigh syndrome and in a *Drosophila* model of familial Parkinson's disease. Thus, mitochondrial retrograde signaling regulates neuronal activity and can be manipulated to enhance neuronal function, despite mitochondrial impairment.

Drosophila | TFAM | HIF alpha | Leigh syndrome | Parkinson's

The human brain constitutes approximately 2% of body weight but consumes 20% of available oxygen because of its high energy demand (1). Mitochondria are abundant in neurons and generate the majority of cellular ATP through the action of the mitochondrial ATP synthase complex. Mitochondrial disorders are one of the most common inherited disorders of metabolism and have diverse symptoms, but tissues with a high metabolic demand, such as the nervous system, are frequently affected (2, 3). The primary insult in all mitochondrial diseases is to mitochondrial function, but the etiology of these diseases is highly pleiotropic (4). This phenomenon is poorly understood, but suggests that the cellular response to mitochondrial dysfunction may be complex and vary between cell types and tissues (4).

Mitochondrial retrograde signaling is defined as the cellular response to changes in the functional state of mitochondria (5). Mitochondrial retrograde signaling enables communication of information about changes in processes such as mitochondrial bioenergetic state and redox potential to the rest of the cell and is thus a key mechanism in cellular homeostasis. The best characterized retrograde responses involve mitochondrial dysfunction eliciting changes in nuclear gene transcription. In yeast, mitochondrial dysfunction causes changes in the expression of genes involved in supplying mitochondria with oxaloacetate and acetyl CoA, the precursors of α-ketoglutarate and glutamate, to compensate for failure of the tricarboxylic acid (TCA) cycle (5). In proliferating mammalian cell models, mitochondrial retrograde signaling is more diverse and involves increases in cytosolic-free Ca^{2+}, leading to activation of Ca^{2+}-responsive calcineurin, causing the up-regulation of genes controlling Ca^{2+} storage and transport (6, 7).

In addition to mitochondrial diseases, alterations in mitochondrial function are also associated with late onset neurodegenerative diseases such as Alzheimer's and Parkinson's (8). Thus, the neuronal response to mitochondrial function may be altered in these diseases and contribute to disease progression. However, neuronal-specific mitochondrial retrograde signaling is poorly understood and its role in neuronal homeostasis is completely unknown. We have developed a neuronal-specific model of mitochondrial dysfunction in *Drosophila* and used this to characterize mitochondrial retrograde signaling in vivo. We show that retrograde signaling regulates neuronal function and can be manipulated to alleviate the effects of mitochondrial dysfunction in neurons.

Results

Tools for Inducing Mitochondrial Dysfunction in *Drosophila*. To develop tools for inducing neuronal-specific mitochondrial dysfunction in *Drosophila* we tested mitochondrial transcription factor A (TFAM) overexpression and expression of a mitochondrially targeted restriction enzyme (mitoXhoI), which cuts the *Drosophila melanogaster* mitochondrial genome once in cytochrome C oxidase (cox) I. TFAM overexpression and mitoXhoI expression have been demonstrated to cause mitochondrial dysfunction in mice and

Significance

Mitochondrial retrograde signaling is an ancient mechanism defined as the cellular response to changes in the functional state of mitochondria. We find that in the *Drosophila* nervous system, mitochondrial dysfunction activates a retrograde response controlling hundreds of nuclear genes. We identify the *Drosophila* ortholog of hypoxia inducible factor alpha (HIFα) as a potential regulator of the neuronal mitochondrial retrograde response. Remarkably, knockdown of HIFα restores neuronal function without affecting the primary mitochondrial defect. Mitochondrial retrograde signaling is therefore partly responsible for neuronal pathology. Knockdown of HIFα also restores function in *Drosophila* models of Leigh syndrome and Parkinson's disease. Our results demonstrate that mitochondrial retrograde signaling has a key role in neuronal homeostasis and that manipulation of retrograde signaling may have therapeutic potential in mitochondrial diseases and Parkinson's.

Author contributions: J.M.B. designed research; U.C., O.F.D., A.P.G., M.S.D., S.T.S., and J.M.B. performed research; U.C., O.F.D., A.P.G., and J.M.B. analyzed data; and J.M.B. wrote the paper.

The authors declare no conflict of interest.

This article is a PNAS Direct Submission.

Data deposition: The data reported in this paper have been deposited in Gene Expression Omnibus (GEO) database, www.ncbi.nlm.nih.gov/geo (accession no. GSE53509).

[1]U.C., O.F.D., and A.P.G. contributed equally to this work.

[2]Present address: Centro Nacional de Investigaciones Cardiovasculares, Melchor Fernández Almagro, 3 Madrid 28029, Spain.

[3]To whom correspondence should be addressed. Email: joseph_matthew.bateman@kcl.ac.uk.

This article contains supporting information online at www.pnas.org/lookup/suppl/doi:10.1073/pnas.1505036112/-/DCSupplemental.

Drosophila, respectively (9, 10). Ubiquitous overexpression of TFAM or expression of mitoXhoI caused early larval or embryonic lethality (*SI Appendix*, Table S1), confirming their deleterious effects.

To further characterize these tools, they were ubiquitously overexpressed in larvae for 3 d, from second to late third instar, using *tub-Gal80^{ts}; tub-Gal4* to overcome the early lethality. Mitochondrial DNA (mtDNA) levels were similar to controls in larvae overexpressing TFAM (Fig. 1*A*). However, levels of the mitochondrially encoded coxI protein were significantly reduced (Fig. 1 *B* and *C*), while levels of nuclear-encoded ATP synthase α were similar to the control (Fig. 1 *B* and *D*). This result suggests that excess TFAM causes mitochondrial dysfunction by inhibiting mitochondrial gene expression, as has been shown previously (10–13). Ubiquitous expression of mitoXhoI for 3 d produced few viable larvae. The few larvae that did survive showed a decrease in mtDNA levels, but this decrease was not significant (Fig. 1*E*). However, using primers that span the XhoI site, mtDNA levels were found to be significantly decreased (Fig. 1*F*), demonstrating that although it does not cause significant mtDNA depletion, mitoXhoI efficiently linearizes the majority of mtDNA by causing a double-stranded break in *coxI*. In conclusion, TFAM overexpression and mitoXhoI expression both cause mtDNA dysfunction in *Drosophila*.

Motor Neuron-Specific Mitochondrial Dysfunction Inhibits Neuronal Function. To determine the consequences of mitochondrial dysfunction in neurons, we used motor neurons, because these are highly accessible to analysis at the cellular and functional level. We used the strong motor neuron driver *OK371-Gal4* to overexpress TFAM or express mitoXhoI and so induce mitochondrial dysfunction specifically in motor neurons. Immunostaining of larval motor neuron cell bodies showed increased TFAM protein expression in TFAM overexpressing cell bodies (*SI Appendix*, Fig. S1*B*). In cell bodies of motor neurons expressing mitoXhoI, TFAM localization was diffuse with fewer TFAM puncta than the control (*SI Appendix*, Fig. S1*C*), suggesting that the expression of mitoXhoI disrupts mtDNA nucleoid morphology.

Motor neuron-specific TFAM overexpression using *OK371-Gal4* caused reduced adult viability at 25 °C (Fig. 2*A* and *SI Appendix*, Table S1), and flies that eclosed died within the first week of life. Enhancing overexpression of TFAM with *OK371-Gal4* by incubation at 29 °C caused late pupal lethality (*SI Appendix*, Table S1). Flies expressing mitoXhoI in motor neurons using *OK371-Gal4* at 25 °C were also late pupal lethal (Fig. 2*A* and *SI Appendix*, Table S1). Thus, both TFAM overexpression

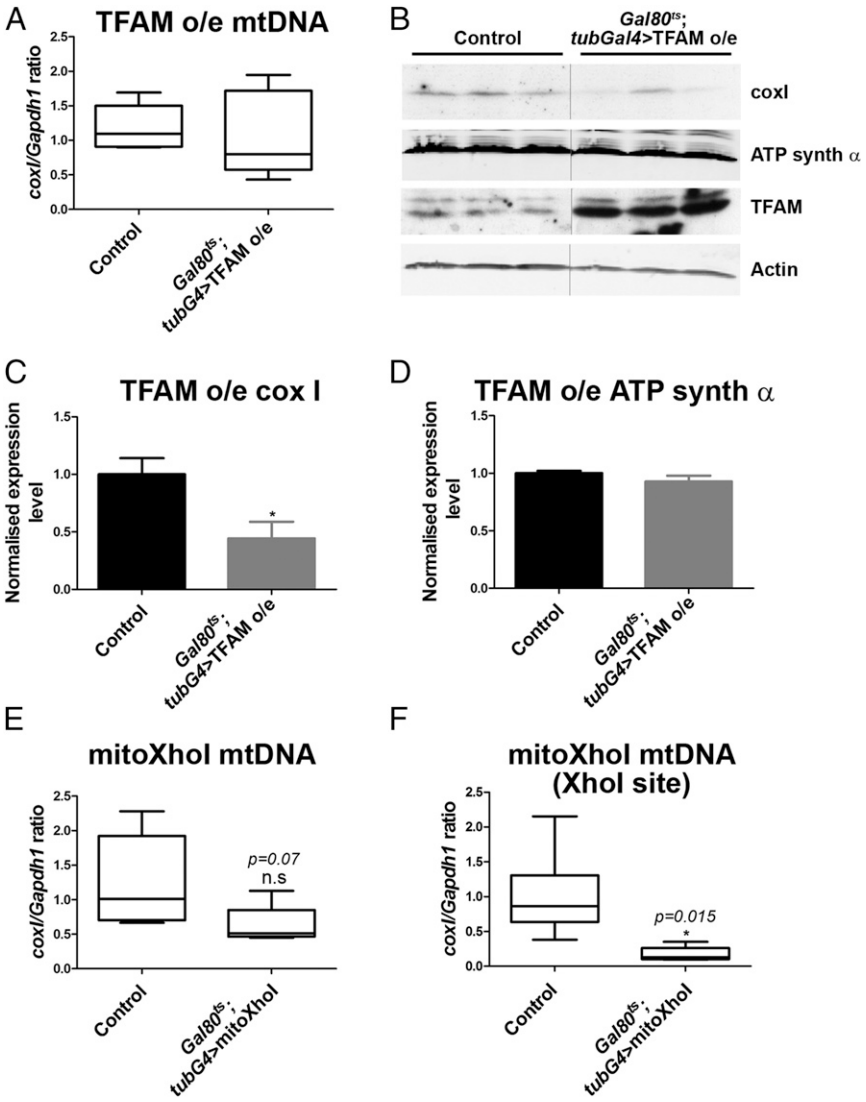

Fig. 1. Tools for inducing mitochondrial dysfunction in *Drosophila*. (*A–D*) Overexpression of TFAM causes reduced mitochondrial gene expression. (*A*) mtDNA levels in late third instar larvae are not significantly different from the control after ubiquitous overexpression of TFAM for 3 d from second to late third instar using *tub-Gal80^{ts}; tub-Gal4*. Control, $n = 8$; TFAM overexpression, $n = 8$. (*B*) Western blot analysis showing the expression of the mitochondrially encoded protein coxI is reduced, but not the nuclear-encoded protein ATP synthase α, in late third instar larvae after ubiquitous overexpression of TFAM for 3 d. Quantification shown in *C* and *D*; control, $n = 3$; TFAM overexpression, $n = 3$. (*E*) mtDNA levels, determined by using standard *coxI* primers, in late third instar larvae are not significantly different from the control after ubiquitous expression of mitoXhoI for 3 d from second to late third instar using *tub-Gal80^{ts}; tub-Gal4*. Control, $n = 7$; mitoXhoI, $n = 5$. (*F*) mtDNA levels determined by using primers spanning the XhoI site in *coxI*, using the same samples as in *E*, are significantly reduced compared with the control. For box and whisker plots, the horizontal line represents the median and whiskers represent the 5th to 95th percentile. For bar graphs, data are represented as mean ± SEM, $*P \leq 0.05$. n.s., not significant. Controls are *tub-Gal80^{ts}; tub-Gal4* hemizygotes.

and mitoXhoI expression in motor neurons affect adult viability, with mitoXhoI causing the stronger phenotype.

Motor neuron-specific TFAM overexpression using *OK371-Gal4* caused a severe decrease in the climbing ability of adult flies (Fig. 2*B*). Use of an independent motor neuron *Gal4* driver (*D42-Gal4*) also resulted in reduced adult climbing with TFAM overexpression (*SI Appendix*, Fig. S1*D*) and lethality with mitoXhoI expression. The *D42-Gal4* driver is also expressed in the crustacean cardioactive peptide (CCAP) neurons that secrete and regulate the release of the neuropeptide bursicon, which activates wing inflation (14, 15). Blocking bursicon release into the hemolymph by inhibition of CCAP neuronal activity causes failure of wing inflation. Overexpression of TFAM using *D42-Gal4* caused failure of wing inflation in approximately 50% of flies (Fig. 2 *C–E*), suggesting that mitochondrial dysfunction causes a partial failure in CCAP neuronal activity. These data show that mitochondrial dysfunction causes defective neuronal function in *Drosophila*.

Motor Neuron Specific Mitochondrial Dysfunction Perturbs Synaptic Development and Causes Loss of Synaptic Mitochondria. To investigate whether mitochondrial dysfunction causes cell death, motor neuron numbers were quantified in the larval CNS. The number of motor neurons was not significantly different from controls in either TFAM-overexpressing or mitoXhoI-expressing larvae (*SI Appendix*, Fig. S2). Moreover, active-caspase 3 expression was similar to controls in the ventral nerve cord (VNC) of larvae overexpressing TFAM or expressing mitoXhoI, or the adult VNC of flies overexpressing TFAM (*SI Appendix*, Fig. S3). Thus, mitochondrial dysfunction does not cause motor neuron cell death in this model. We therefore focused on the neuromuscular junction (NMJ) as a compartment that could potentially be adversely affected by mitochondrial dysfunction.

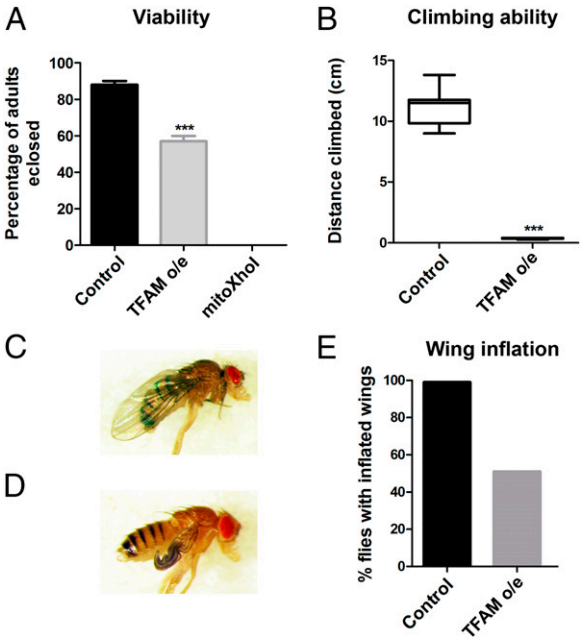

Fig. 2. Motor neuron-specific mitochondrial dysfunction reduces viability, locomotor activity, and wing inflation. (*A*) Overexpression of TFAM, or expression of mitoXhoI in motor neurons using *OK371-Gal4* causes reduced adult viability and pupal lethality, respectively. (*B*) Motor neuron-specific TFAM overexpression using *OK371-Gal4* severely decreases adult climbing ability (mitoXhoI expression causes late pupal lethality so could not be tested). (*C* and *D*) Overexpression of TFAM using *D42-Gal4* causes defective wing inflation (*D*), compared with the control (*C*). (*E*) Quantification of the wing inflation phenotype. Control, $n = 99$; TFAM overexpression, $n = 51$. For box and whisker plot, the horizontal line represents the median and whiskers represent the 5th to 95th percentile. The bar graph data in *A* are represented as mean ± SEM, $***P \leq 0.001$. Controls are *Gal4* hemizygotes.

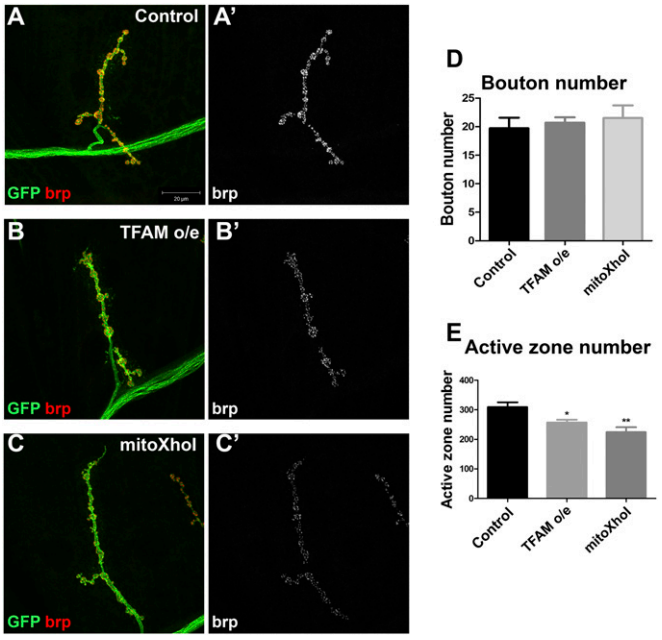

Fig. 3. Motor neuron-specific mitochondrial dysfunction causes defective active zone development. (*A–C*) Hemisegment A3, muscle 4 NMJ in late third instar larvae from control (*A*), larvae overexpressing TFAM (*B*), or larvae-expressing mitoXhol (*C*) in motor neurons using *OK371-Gal4*. Expression of CD8-GFP (GFP, green) was used to visualize neuronal membranes and brp staining (red in *A–C* and white in *A′–C′*) to visualize active zones. (*D* and *E*) Quantification of bouton number (*D*) and active zone number (*E*). Data are represented as mean ± SEM, $*P \leq 0.05$, $**P \leq 0.01$. Controls are *OK371-Gal4* hemizygotes.

Bouton numbers were similar to controls at the muscle 4 hemisegment A3 NMJ of TFAM-overexpressing or mitoXhoI-expressing motor neurons, establishing that overall neuronal morphology is unaffected by mitochondrial dysfunction (Fig. 3 *A–D*). However, the number of active zones (the sites of neurotransmitter release), as assessed by staining for the active zone protein bruchpilot (brp), were significantly reduced in NMJs under both conditions (Fig. 3 *A–C* and *E*). Similar results were found for the muscle 6/7 NMJ (*SI Appendix*, Fig. S4). These data suggest that mitochondrial dysfunction resulting from overexpression of TFAM, or expression of mitoXhoI, perturbs active zone development.

Mitochondria are abundant at the synapse, and presynaptic mitochondrial function is essential for efficient neurotransmitter release. Live imaging of presynaptic mitochondria stained with the vital dye tetramethylrhodamine methyl ester (TMRM) showed a striking decrease in the abundance of mitochondria in motor neurons overexpressing TFAM or expressing mitoXhoI, compared with controls (*SI Appendix*, Fig. S5 *A–C*). TMRM intensity in these mitochondria was similar to controls (*SI Appendix*, Fig. S5*D*), suggesting the remaining mitochondria are functional. The reduction in mitochondria in TFAM-overexpressing or mitoXhoI-expressing NMJs was also observed with the membrane potential-independent dye Mitotracker Green (*SI Appendix*, Fig. S5 *E–G*). To quantify this phenotype, mitochondria at muscle 4 NMJ were imaged in fixed tissue by using a mitochondrially targeted GFP expressed in motor neurons. Quantitative analysis revealed a severe decrease in mitochondrial number and volume under both conditions (Fig. 4 *B–E*). Therefore, mitochondrial dysfunction induced by overexpression of TFAM or expression of mitoXhoI in motor neurons causes a dramatic reduction in mitochondria at the NMJ. In neurons expressing either of these tools, individual NMJ mitochondria appeared similar to the control at the ultrastructural

level (Fig. 4 *F–H*), suggesting that mitochondrial dysfunction does not affect the gross internal structure of presynaptic mitochondria.

We next asked whether mitochondria in other parts of the motor neuron are affected by overexpression of TFAM or mitoXhoI expression. Under both conditions motor neuron cell body mitochondria were much less reticular and had a more punctate morphology than in control neurons (*SI Appendix*, Fig. S6 *A–C*). In the proximal axon, mitochondrial numbers were similar to the control in TFAM-overexpressing motor neurons, but were significantly reduced in neurons expressing mitoXhoI (*SI Appendix*, Fig. S6 *D–F* and *J*). Mitochondrial volume in the proximal axon was similar to the control in both TFAM-overexpressing and mitoXhoI-expressing motor neurons (*SI Appendix*, Fig. S6 *D–F* and *K*). A much stronger affect was observed in the distal axon, where mitochondrial number and volume were both significantly reduced by TFAM overexpression and mitoXhoI expression (*SI Appendix*, Fig. S6 *G–I*, *L*, and *M*). In summary, these data show that mitochondrial dysfunction causes a progressive loss of mitochondria from the proximal to distal axonal compartment and at synapses in motor neurons.

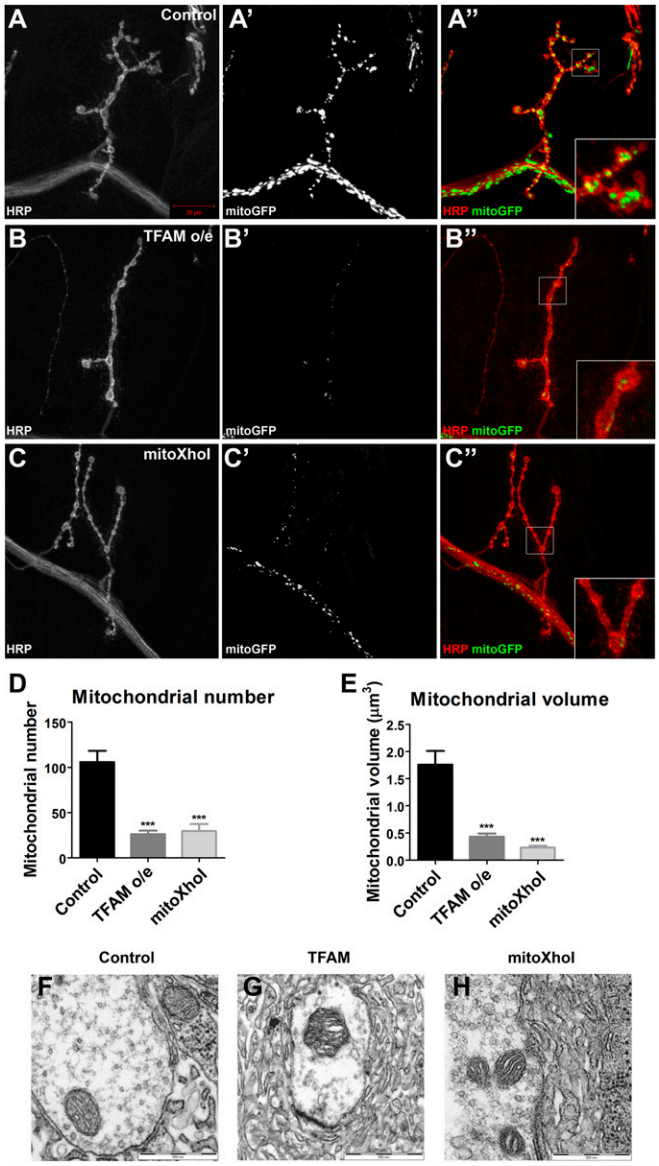

Fig. 4. Mitochondrial dysfunction causes loss of synaptic mitochondria. Hemisegment A3, muscle 4 NMJ in late third instar larvae from control (*A*), larvae overexpressing TFAM (*B*), or larvae expressing mitoXhoI (*C*) in motor neurons using *OK371-Gal4*. Motor neuron-specific expression of mitoGFP (white in *A′–C′* and green in A′′–*C′′*) was used to visualize mitochondria and staining for horseradish peroxidize (HRP, white in *A–C* and red in A′′–*C′′*) to visualize neuronal membranes. (*D* and *E*) Quantification of mitochondrial number and volume. (*F–H*) TEM images of mitochondria in muscle 6/7 NMJs from control (*F*), TFAM overexpressing (*G*), and mitoXhoI-expressing (*H*) late third instar motor neurons using *OK371-Gal4*. Data are represented as mean ± SEM, ***$P \leq 0.001$. Controls are *OK371-Gal4* hemizygotes.

Reduced Mitochondrial Glutathione Redox Potential in Neurons with Mitochondrial Dysfunction. Mitochondria are the main source of intracellular reactive oxygen species (ROS). Superoxide, created by the mitochondrial electron transport chain, is converted to hydrogen peroxide, which is then scavenged by glutathione (4). To determine the effects of neuronal mitochondrial dysfunction on glutathione redox potential, we used a genetically encoded ratiometric fluorescent probe (mito-roGFP2-Grx1) (16) expressed in motor neurons. We imaged mito-roGFP2-Grx1 fluorescence at the larval NMJ and found that mitochondrial dysfunction, caused by the overexpression of TFAM or expression of mitoXhoI, resulted in a significant decrease in probe oxidation (*SI Appendix*, Fig. S7 *A–G*). These data indicate that neuronal mitochondrial dysfunction causes reduced mitochondrial ROS levels.

Neuronal Mitochondrial Dysfunction Activates a Mitochondrial Retrograde Response. To investigate the mitochondrial retrograde response to neuronal mitochondrial dysfunction, we performed microarray gene expression analysis from late third instar larval CNS tissue. To avoid the need to isolate specific neuronal subtypes, the pan-neuronal *nSyb-Gal4* driver was used to drive expression in all differentiated neurons throughout the CNS. Overexpression of TFAM with *nSyb-Gal4* caused late pupal lethality, whereas expression of mitoXhoI with *nSyb-Gal4* produced few third instar larvae. As an alternative to mitoXhoI, we used RNAi to knockdown the expression of mitochondrial *ATP synthase subunit F6* (*ATPsynCF6*). Subunit F6 (encoded by *ATP5J* in humans) is a component of the F0 complex of mitochondrial ATP synthase (complex V) and part of the peripheral stalk that links the F0 and F1 complexes and is critical for ATP synthase function (17). Ubiquitous *ATPsynCF6* RNAi caused an ∼90% reduction in *ATPsynCF6* expression (*SI Appendix*, Fig. S8*A*). Similar to TFAM overexpression, motor neuron-specific RNAi of *ATPsynCF6* causes defects in adult climbing and wing inflation, loss of synaptic mitochondria, and altered glutathione redox potential (*SI Appendix*, Fig. S8 *B–L*). RNAi of *ATPsynCF6* with *nSyb-Gal4* also caused pupal lethality.

Microarray analysis of larval CNS tissue showed that the expression of 294 genes were significantly changed in TFAM overexpressing tissue, while 371 genes were significantly changed in *ATPsynCF6* RNAi tissue (Fig. 5*A* and Datasets S1 and S2). Approximately half (142) of the genes whose expression was significantly changed in TFAM-overexpressing tissue were also significantly changed in *ATPsynCF6* RNAi tissue (Fig. 5*A* and Dataset S3), and there was a strong positive correlation between the expression changes of these genes under the two conditions ($r = 0.93$, $P < 0.0001$; Fig. 5*B*) Therefore, neuronal mitochondrial dysfunction caused either by TFAM overexpression or *ATPsynCF6* RNAi results in distinct but overlapping mitochondrial retrograde responses. Gene ontology (GO) analysis determined that the genes regulated in TFAM overexpression or *ATPsynCF6* RNAi CNS tissue are significantly enriched for several GO terms including transcriptional regulation, ribosomal subunit, ribonucleotide binding, and chromosome organization (*SI Appendix*, Figs. S9–S11). Furthermore, *Impl3,* encoding lactate dehydrogenase and *Tret1-1,* encoding the trehalose transporter (trehalose is the primary circulating sugar in insects), were two of the most strongly increased genes in both TFAM overexpression and *ATPsynCF6* RNAi tissue (*SI Appendix*, Table S2 and Datasets S1 and S2). These data suggest a compensatory response to mitochondrial dysfunction involving increased trehalose uptake and glycolysis.

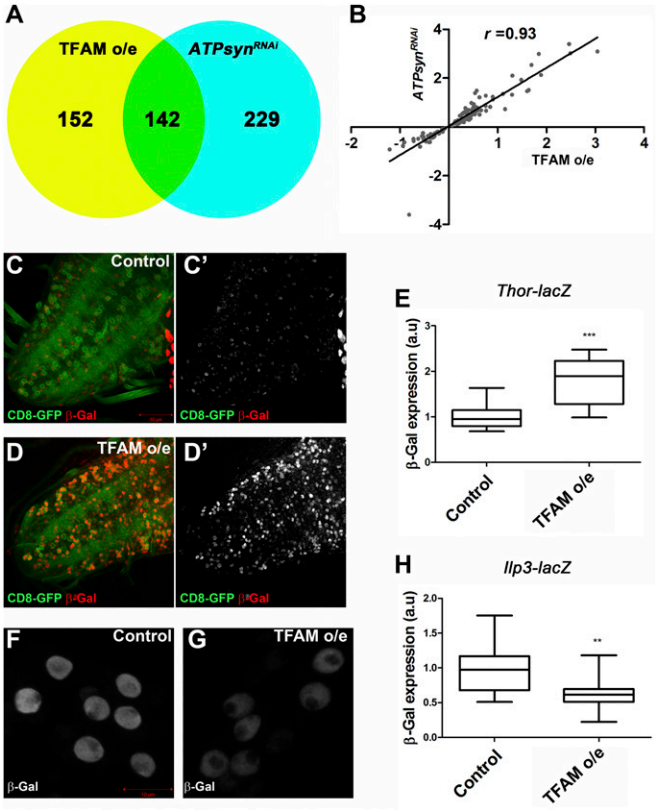

Fig. 5. Neuronal mitochondrial dysfunction activates a retrograde response. (*A*) Venn diagram showing the numbers of genes with significantly altered expression from larval CNS tissue with mitochondrial dysfunction caused by overexpression of TFAM or RNAi of *ATPsynCF6* using *nSyb-Gal4*. (*B*) Scatter plot showing the correlation between genes with significantly altered expression in the two genotypes. (*C–D′*) *Thor-lacZ* expression (red in *C* and *D* and white in *C′* and *D′*) in the VNC of a control larva or a larva overexpressing TFAM in motor neurons using *OK371-Gal4*. CD8-GFP expression (green) shows the *OK371-Gal4* expression pattern in motor neurons. (*E*) Quantification of *Thor-lacZ* expression in motor neuron cell bodies. Control, $n = 21$; TFAM overexpression, $n = 16$. (*F* and *G*) *Ilp3-lacZ* expression in the median neurosecretory neurons from a control larva (*F*), or a larva overexpressing TFAM in neurons using *nSyb-Gal4* (*G*). (*H*) Quantification of *Ilp3-lacZ* expression in the median neurosecretory neurons. Control, $n = 15$; TFAM overexpression, $n = 20$. a.u., arbitrary units. For box and whisker plots, the horizontal line represents the median and whiskers represent the 5th to 95th percentile. $^{**}P \leq 0.01$, $^{***}P \leq 0.001$. Controls are *Gal4* hemizygotes.

The expression of *Thor*, encoding the eukaryotic initiation factor 4E binding protein (4E-BP), was also highly up-regulated in both TFAM overexpression and *ATPsynCF6* RNAi CNS tissue (*SI Appendix*, Table S2 and Datasets S1 and S2). 4E-BP is a key negative regulator of insulin receptor (InR)/mechanistic target of rapamycin (mTOR) signaling, acting downstream of mTORC1 (18). Expression of one of the seven *Drosophila* insulin-like peptides (*Ilp1*) was significantly decreased in TFAM overexpressing CNS tissue (*SI Appendix* and Dataset S1), while the expression of both *Ilp1* and *Ilp3* were significantly decreased in *ATPsynCF6* RNAi tissue (*SI Appendix* and Dataset S2). The expression of *Ilp3* was also decreased in TFAM overexpressing tissue, but fell below the cutoff used to be considered significantly changed. Using a *lacZ* enhancer trap in *Thor*, we found that *Thor* is normally weakly expressed in motor neurons, but overexpression of TFAM in motor neurons using *OK371-Gal4* caused a significant increase in *Thor-lacZ* expression (Fig. 5 *C–E*). A *lacZ* enhancer trap in *Ilp3* is strongly expressed in the seven median neurosecretory neurons in the central brain (Fig. 5*F*). Overexpression of TFAM using *nSyb-Gal4* caused a significant decrease in *Ilp3-lacZ* expression in the median neurosecretory neurons (Fig. 5 *F–H*). These data confirm that mitochondrial dysfunction modulates the transcription of retrograde response genes in the *Drosophila* CNS.

We also compared the 142 genes that are commonly regulated by TFAM overexpression and *ATPsynCF6* RNAi to those regulated in three other *Drosophila* models of mitochondrial dysfunction. *Impl3* expression is significantly increased in *tko* mutant flies, *pink1* mutant flies, and cytochrome *c* oxidase Va (CoVa) knock-down S2 cells, while *Thor* expression is significantly increased in the latter two models (Dataset S4) (19–21). Overall, although different tissues were used, 31 genes were commonly regulated in our gene set and at least one of the other three studies (Dataset S4). Comparison of these different models thus demonstrates that there are a common set of mitochondrial retrograde response genes.

Modulation of Mitochondrial Retrograde Signaling via Knockdown of HIFα Improves Neuronal Function. The transcription factor hypoxia inducible factor (HIF) is the main sensor of cellular oxygen levels and shifts cells to a glycolytic state during hypoxia (22). There is a small significant increase in the expression of the *Drosophila HIFα* ortholog *similar* (*sima*) in TFAM-overexpressing CNS tissue (Dataset S1), and an increase in *ATPsynCF6* RNAi CNS tissue, but this increase fell below the cutoff used to be considered significantly changed. The glucose transporter *Glut-1* is a direct target of HIF1α in mammalian cells (23), while *LDHA* and *Impl3* (encoding LDH in *Drosophila*) are direct transcriptional targets of HIFα in mammalian cells and *Drosophila*, respectively (24, 25). The HIFα-dependent transcriptional response has been characterized in *Drosophila* larvae (26). The genes regulated in both TFAM-overexpressing and *ATPsynCF6* RNAi CNS tissue show a significant overlap with HIFα-regulated genes, including *Impl3* and *Thor* ($P < 0.0001$; Dataset S4). We directly tested whether Sima regulates other mitochondrial retrograde response genes in addition to *Impl3*. Overexpression of Sima in motor neurons caused a strong increase in *Thor-lacZ* expression (Fig. 6 *A–C*), demonstrating that Sima positively regulates *Thor* transcription. Moreover, overexpression of Sima using *nSyb-Gal4* caused a significant decrease in the expression of *Ilp3-lacZ* in the median neurosecretory neurons (Fig. 6 *D–F*). These data are consistent with Sima acting as a regulator of neuronal mitochondrial retrograde signaling in the *Drosophila* nervous system.

To test whether Sima is required for the neuronal mitochondrial retrograde response we analyzed the effect of TFAM overexpression on *Thor-lacZ* in motor neurons expressing a short hairpin RNA (shRNA) targeting *sima*. Ubiquitous expression of this shRNA (HMS00833) caused an ∼65% decrease in *sima* expression (*SI Appendix*, Fig. S12*A*). Knockdown of Sima in motor neurons restored the up-regulation of *Thor-lacZ* caused by TFAM overexpression to control levels (Fig. 6 *G–K*). Therefore, Sima is required for the positive regulation of *Thor* expression via neuronal mitochondrial retrograde signaling.

To determine whether modulation of mitochondrial retrograde signaling affects neuronal function, we induced mitochondrial dysfunction by overexpressing TFAM in motor neurons and simultaneously either overexpressed or knocked down Sima. Overexpression of Sima in motor neurons using *D42-Gal4* caused a significant decrease in climbing ability, but did not alter the climbing ability of flies overexpressing TFAM (Fig. 7*A*). By contrast, knockdown of Sima significantly improved the reduced climbing ability caused by TFAM overexpression in motor neurons using *D42-Gal4* (Fig. 7*B*). Knockdown of Sima also rescued the late pupal lethality caused by overexpression of TFAM in motor neurons by using *OK371-Gal4* at 29 °C (*SI Appendix*, Table S1). Furthermore, knockdown of Sima completely suppressed the wing inflation defect caused by TFAM overexpression by using *D42-Gal4* ($P < 0.0001$; Fig. 7*C*). A similar degree of Sima knockdown and rescue of TFAM overexpression phenotypes was obtained by using an independent shRNA (HMS00832) against *sima* (*SI Appendix*, Fig. S12). Overexpression

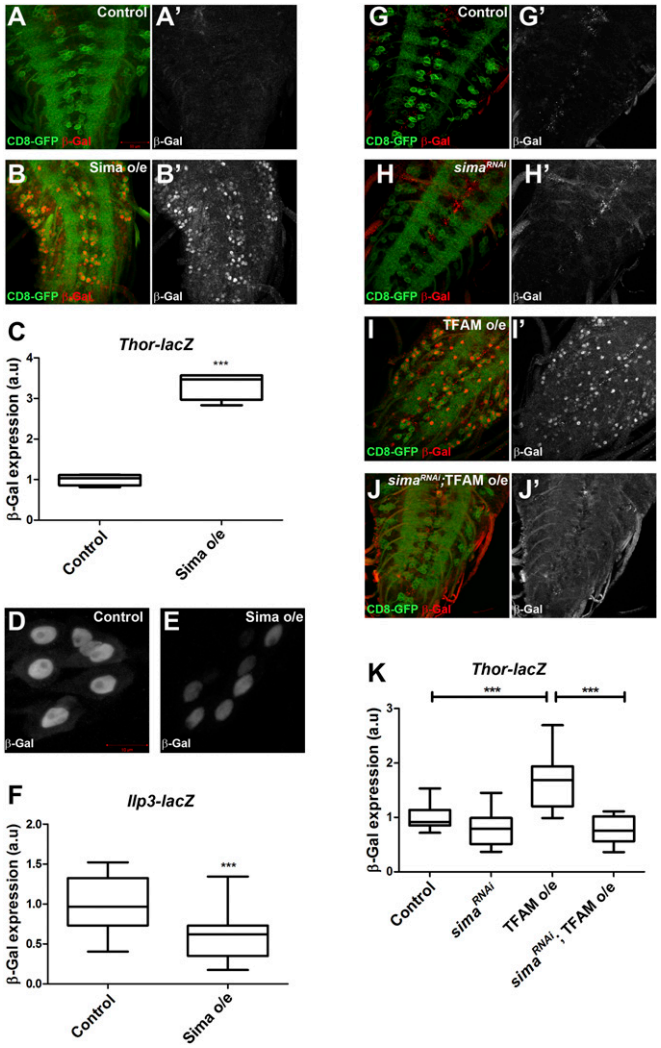

Fig. 6. Sima is required for increased *Thor* expression in response to mitochondrial dysfunction. (*A* and *B*) *Thor-lacZ* (red in *A* and *B*, white in *A′* and *B′*) expression is strongly increased in motor neurons overexpressing Sima (*B* and *B′*) using *OK371-Gal4* compared with the control (*A* and *A′*). (*C*) Quantification of *Thor-lacZ* expression. Control, $n = 4$; Sima overexpression, $n = 4$. (*D* and *E*) *Ilp3-lacZ* expression is reduced in median neurosecretory neurons overexpressing Sima (*E*), compared with the control (*D*). (*F*) Quantification of *Ilp3-lacZ* expression. Control, $n = 18$; Sima overexpression, $n = 22$. (*G–J*) The increase in *Thor-lacZ* expression (red in *G–J* and white in *G′–J′*) caused by TFAM overexpression (*I* and *I′*) is abrogated by RNAi of *sima* (*J* and *J′*). (*K*) Quantification of *Thor-lacZ* expression. Control, $n = 10$; *sima* RNAi, $n = 10$; TFAM overexpression, $n = 12$; *sima* RNAi;TFAM overexpression, $n = 13$. CD8-GFP expression (green in *A*, *B*, and *G–J*) shows the *OK371-Gal4* expression pattern in motor neurons. a.u., arbitrary units. For box and whisker plots, the horizontal line represents the median and whiskers represent the 5th to 95th percentile. $***P \leq 0.001$. Controls are *Gal4* hemizygotes.

of TFAM with *OK371-Gal4* causes reduced viability (Fig. 2*A*) and severely reduced lifespan, whereas TFAM overexpression with *D42-Gal4* causes adult flies to live about half as long as controls (Fig. 7*D*). This reduced lifespan was almost completely rescued by knockdown of Sima (Fig. 7*D* and *SI Appendix*, Tables S3 and S4). Knockdown of Sima with *D42-Gal4* also almost completely suppressed the wing inflation defect caused by *ATPsynCF6* RNAi ($P < 0.0001$), but it did not rescue the strong climbing phenotype (*SI Appendix*, Fig. S13 *A* and *B*). Therefore, inhibition of mitochondrial retrograde signaling by knockdown of Sima at least partially prevents the neuronal functional defects caused by mitochondrial dysfunction.

To investigate the basis for the improvement in neuronal function caused by Sima knockdown, we analyzed the NMJ of motor neurons overexpressing TFAM and *sima* shRNA. Knockdown of Sima alone caused a moderate but significant decrease in NMJ mitochondrial number and volume, but did not affect the reduction in mitochondrial number and volume caused by TFAM overexpression (Fig. 7*E* and *SI Appendix*, Fig. S13 *C–G*). However, Sima knockdown restored the reduction in active zone number caused by TFAM overexpression to wild-type levels (Fig. 7*F* and *SI Appendix*, Fig. S13 *H–K*). Thus, the beneficial effects of Sima knockdown on neuronal function may be due to suppression of the defect in active zone development caused by mitochondrial dysfunction.

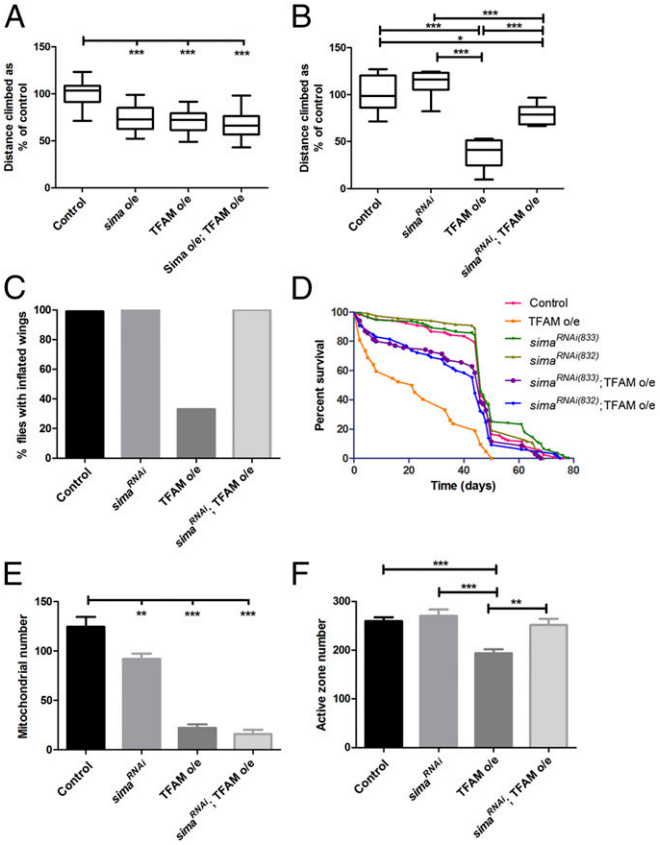

Fig. 7. Knockdown of Sima improves the function of neurons with mitochondrial dysfunction. (*A*) Overexpression of Sima does not affect the climbing defect caused by overexpression of TFAM in motor neurons using *D42-Gal4*. Note that a TFAM insertion on the third chromosome (TFAM10M) was used in this experiment, which gives a weaker climbing phenotype than the TFAM insertion on the second chromosome (TFAM3M) used elsewhere. (*B*) Knockdown of Sima (using shRNA HMS00833) dramatically improves the climbing ability of flies overexpressing TFAM using *D42-Gal4*. (*C*) Knockdown of Sima (using shRNA HMS00833) rescues the wing inflation defect of flies overexpressing TFAM using *D42-Gal4* ($P < 0.0001$). Control, $n = 187$; *sima* RNAi, $n = 97$; TFAM overexpression, $n = 47$; *sima* RNAi;TFAM overexpression, $n = 95$. (*D*) Lifespan analysis of flies overexpressing TFAM in motor neurons, using *D42-Gal4*, alone, or in combination with two independent shRNAs targeting *sima*. See *SI Appendix*, Tables S3 and S4 for statistical analysis. (*E*) Knockdown of Sima (using shRNA HMS00833) does not affect the reduction in larval NMJ mitochondrial number caused by overexpression of TFAM using *OK371-Gal4*. (*F*) Knockdown of Sima (using shRNA HMS00833) rescues the reduction in larval NMJ active zone number caused by overexpression of TFAM using *OK371-Gal4*. For box and whisker plots, the horizontal line represents the median and whiskers represent the 5th to 95th percentile. For bar graphs in *E* and *F*, data are represented as mean ± SEM, $*P \leq 0.05$, $**P \leq 0.01$, $***P \leq 0.001$. Controls are *Gal4* hemizygotes.

Knockdown of HIFα Improves Function in *Drosophila* Models of Leigh Syndrome and Parkinson's Disease. We next tested whether knockdown of Sima is beneficial in *Drosophila* models of mitochondrial disease. Human mitochondrial complex IV (COX) deficiency has been associated with mutations in several nuclear and mitochondrially encoded genes (27). The pupal lethality caused by a temperature-sensitive mutation in the mitochondrial gene *coxI* (28) was not rescued by either ubiquitous (*Da-Gal4*) or pan-neuronal (*nSyb-Gal4*) Sima knockdown. Mutations in the nuclear gene *Surf1*, encoding a COX assembly factor, cause the childhood encephalomyelopathy Leigh syndrome (29, 30). Pan-neuronal knockdown of Surf1 with *nSyb-Gal4*, using a previously validated double-stranded RNA (31), caused reduced climbing ability and defective wing inflation (Fig. 8 *A*–*C*). Simultaneous knockdown of Surf1 and Sima caused a complete rescue of the Surf1 RNAi climbing phenotype in female flies and a strong suppression in males (Fig. 8 *A* and *B*). *sima* RNAi also completely rescued the wing inflation defect caused by knockdown of Surf1 ($P < 0.0001$; Fig. 8*C*). Therefore, reducing Sima expression is beneficial in a *Drosophila* mitochondrial disease model.

Mutations in the ubiquitin ligase Parkin cause autosomal recessive juvenile parkinsonism, a familial form of Parkinson's disease. *Drosophila parkin* mutants have mitochondrial defects and reduced climbing ability (32). Ubiquitous knockdown of Sima using *Da-Gal4* significantly improved the climbing ability of $park^{25}$ mutant flies, even though ubiquitous *sima* RNAi alone caused reduced climbing ability (Fig. 8*D*). Thus, knockdown of Sima at least partially restores function in a *Drosophila* Parkinson's disease model.

Discussion

We have developed a model of neuronal-specific mitochondrial dysfunction in *Drosophila*. Using this model, we have analyzed the effects of mitochondrial dysfunction in neurons at the cellular and functional level. We have analyzed global changes in nuclear gene expression and find that there is a retrograde response to neuronal mitochondrial dysfunction in the *Drosophila* CNS. We show that the *Drosophila* HIFα ortholog Sima is potentially a key regulator of the mitochondrial retrograde response in the nervous system and that knockdown of Sima dramatically improves neuronal function in this and other models of mitochondrial dysfunction. Surprisingly, Sima activity in part causes the dysfunction of neurons containing defective mitochondria.

Previous studies of *Drosophila* mutants in the regulatory and catalytic subunits of the mitochondrial DNA polymerase Polγ have demonstrated that loss of mtDNA replication in *Drosophila* causes mtDNA loss, reduced neuronal stem cell proliferation, and developmental lethality (33, 34). To avoid the pleiotropic effects of using homozygous mutant animals, we developed a neuronal-specific model of mitochondrial dysfunction. We characterized the phenotypes resulting from TFAM overexpression and expression of a mitochondrially targeted restriction enzyme and found that both of these tools can be used to model neuronal-specific mitochondrial dysfunction. Overexpression of TFAM results in mitochondrial dysfunction caused by inhibition of mitochondrial gene expression, rather than an alteration in mtDNA copy number. Overexpression of TFAM has been shown to have different effects depending on the cell type, model system, or ratio of TFAM protein to mtDNA copy number (10–13, 35). Our results are consistent with in vitro studies and overexpression of human TFAM in mice and human cells, which have shown that excess TFAM results in the suppression of mitochondrial gene transcription (10–13).

We found that ubiquitous expression of mitoXhoI causes early developmental lethality and that, although there was no significant mtDNA loss, the majority of mtDNA was linearized. Given that mtDNA is transcribed as two polycistronic mRNAs, a

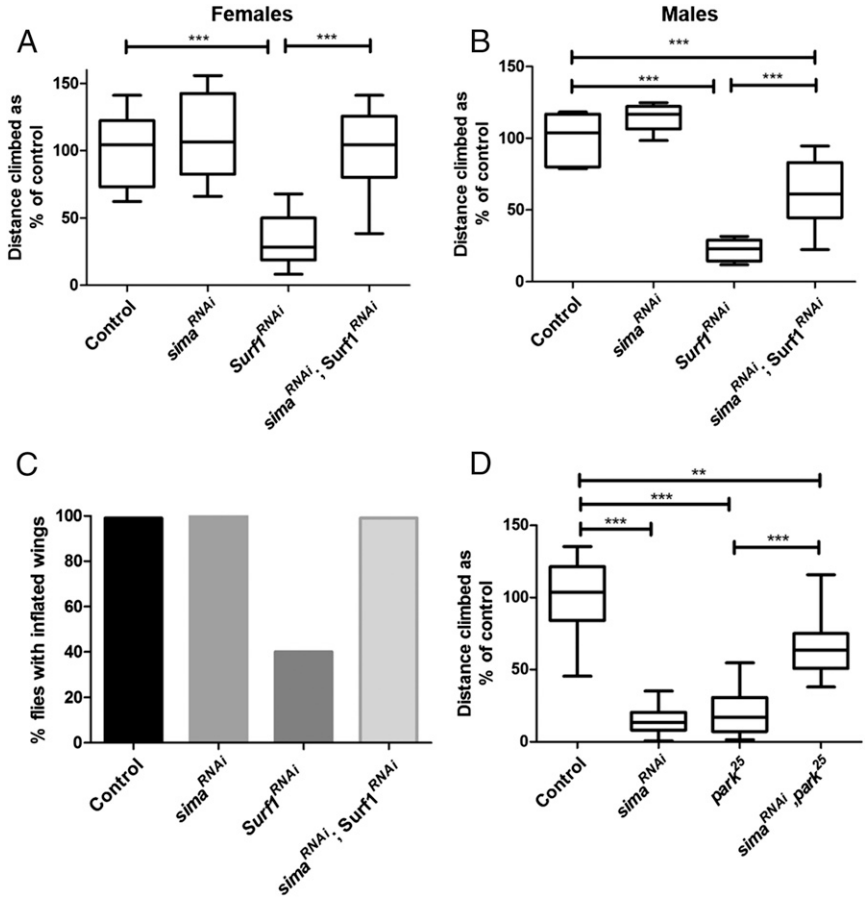

Fig. 8. Sima knockdown improves function in *Drosophila* models of Leigh syndrome and Parkinson's disease. (*A* and *B*) Pan-neuronal RNAi of *Surf1* using *nSyb-Gal4* causes reduced climbing ability, but this phenotype is completely rescued in female flies (*A*) and partially rescued in male flies (*B*) by knockdown of Sima. (*C*) Pan-neuronal RNAi of *Surf1* using *nSyb-Gal4* causes defective wing inflation, but this defect is completely rescued by knockdown of Sima ($P < 0.0001$). Control, $n = 185$; *sima* RNAi, $n = 152$; *Surf1* RNAi, $n = 67$; *sima* RNAi, *Surf1* RNAi $n = 208$. (*D*) The climbing defect in $park^{25}$ male flies is partially restored by ubiquitous knockdown of Sima using *Da-Gal4*. For box and whisker plots, the horizontal line represents the median and whiskers represent the 5th to 95th percentile. $^{**}P \leq 0.01$, $^{***}P \leq 0.001$. Controls are *Gal4* hemizygotes.

double-stranded break in *coxI* would block the transcription of the majority of mitochondrially encoded genes, resulting in severe mitochondrial dysfunction.

Using a *Drosophila* motor neuron model, we found that mitochondrial dysfunction caused a reduction in the number of active zones, loss of synaptic mitochondria, and locomotor defects. Mitochondrial dysfunction caused by overexpression of PINK1 or Parkin decreases the rate of mitochondrial transport in vitro and in vivo (36). Furthermore, a recent study using KillerRed demonstrated that local mitochondrial damage results in mitophagy in axons (37). Therefore, the acute loss of synaptic mitochondria in our model may result from defects in mitochondrial transport and/or mitophagy.

Previous studies in mice have examined the effects of neuronal mitochondrial dysfunction by using mitoPstI expression, or targeted knockout of TFAM (38, 39). Knockout of TFAM specifically in mouse dopaminergic neurons (the "MitoPark" mouse model) causes progressive loss of motor function, intraneuronal inclusions, and eventual neuronal cell death (38, 40). Interestingly, cell body mitochondria are enlarged and fragmented and striatal mitochondria are reduced in number and size in MitoPark dopaminergic neurons (41), suggesting that the effects of neuronal mitochondrial dysfunction are conserved in *Drosophila* and mammals.

Larvae mutant for the mitochondrial fission gene *drp1* have fused axonal mitochondria and almost completely lack mitochondria at the NMJ (42), similar to motor neurons overexpressing TFAM or expressing mitoXhoI. Adult *drp1* mutant flies also have severe behavioral defects. Synaptic reserve pool vesicle mobilization is inhibited in *drp1* mutant larvae because of the lack of ATP to power the myosin ATPase required for reserve pool tethering and release. Reserve pool vesicle mobilization is likely to be similarly affected in TFAM overexpressing or mitoXhoI-expressing motor neurons, which would result in locomotor defects in these animals. Interestingly, expression of the Arctic form of β-amyloid$_{1–42}$ (Aβ) in *Drosophila* giant fiber neurons also leads to the depletion of synaptic mitochondria and decreased synaptic vesicles (43). Synaptic loss and alterations in neuronal mitochondrial morphology have also been observed in postmortem tissue from Alzheimer's disease patients (44, 45). The parallels between these phenotypes and those in our model suggest a common underlying mechanism.

Using microarray analysis, we find that mitochondrial dysfunction in neurons regulates the expression of hundreds of nuclear genes. The *Drosophila* CNS contains different neuronal subtypes, and glial cells, so the results of the microarray are heterogeneous, representing the pooled response to mitochondrial dysfunction throughout the CNS. We have phenotypically characterized mitochondrial dysfunction in motor neurons, but not all of the genes identified from the microarrays are expressed in motor neurons, e.g., *Ilp3*. The specific genes that are regulated differ depending on whether mitochondrial dysfunction results from TFAM overexpression or knockdown of ATPsynCF6. However, a core group of approximately 140 genes are similarly regulated in both conditions. Yeast mutants in different components of the TCA cycle result in differing retrograde responses (46) and comparison of somatic cell hybrids (cybrids) carrying the A3243G mtDNA mutation with cybrids completely lacking mtDNA (ρ^0 cells) showed overlapping but distinct gene expression profiles (47). Moreover, a later study comparing cybrids with increasing levels of the A3243G mtDNA mutation showed markedly different alterations in nuclear gene expression, depending on the severity of mitochondrial dysfunction (48). Taken together, these data suggest that the cellular response to mitochondrial dysfunction is not uniform and adapts to the specific defect and severity of the phenotype. Therapeutic strategies targeting mitochondrial dysfunction in human disease may therefore need to be tailored to the specific mitochondrial insult.

Concomitant with our findings, previous studies have shown that in yeast, *Drosophila*, and mammalian-proliferating cells, retrograde signaling activates the expression of hypoxic/glycolytic genes and the insulin-like growth factor-1 receptor pathway to compensate for mitochondrial dysfunction (20, 46, 49). Rtg1 and Rtg3, the transcription factors that coordinate the mitochondrial retrograde response in yeast, are not conserved in metazoans. In mammalian proliferating cellular models, the retrograde response activates the transcription factors nuclear factor of activated T cells (NFAT), CAAT/enhancer binding protein δ (C/EBPδ), cAMP-responsive element binding protein (CREB), and an IκBβ-dependent nuclear factor κB (NFκB) c-Rel/p50 (49–51). Whether these transcription factors regulate mitochondrial retrograde signaling in the mammalian nervous system is not known.

HIFα/Sima is a direct regulator of *LDH* expression in flies and mammals, and we find that Sima also regulates the expression of two other retrograde response genes, *Thor* and *Ilp3*, in the *Drosophila* nervous system. Importantly, Sima is required for the increase in *Thor* expression in response to mitochondrial dysfunction. Sima has been strongly implicated as a key regulator of mitochondrial retrograde signaling in *Drosophila* S2 cells knocked down for the gene encoding subunit Va of complex IV (20). *sima*, *Impl3*, and *Thor* expression were all increased in this model, and there is a significant overlap with the genes regulated in our model ($P < 0.0001$; Dataset S4). These data support the possibility that the *Drosophila* HIFα ortholog Sima is a key transcriptional regulator of neuronal mitochondrial retrograde signaling.

HIFα is stabilized in hypoxia through the action of prolyl hydroxylases (22) and this mechanism was thought to require ROS, but HIFα stabilization may in fact be ROS independent (52, 53). In mammalian cells carrying the mtDNA A1555G mutation in the 12S rRNA gene, mitochondrial retrograde signaling has been shown to be activated by increased ROS, acting through AMPK and the transcription factor E2F1 to regulate nuclear gene expression (54). In the *Drosophila* eye, loss of the complex IV subunit *cytochrome c oxidase Va* (*CoVa*) causes decreased ROS (55). However, retrograde signaling upon loss of *CoVa* was not mediated by decreased ROS, but by increased AMP activating AMPK. Similarly, the small decrease in redox potential in neurons in response to mitochondrial dysfunction in our model makes it unlikely that ROS are the mediator of the retrograde signal. Moreover, HIFα physically interacts with several transcriptional regulators including the *Drosophila* and mammalian estrogen-related receptor and Smad3, as well as its heterodimeric binding partner HIFβ, to regulate gene expression (22, 26, 56, 57). Mitochondrial retrograde signaling may modulate these or other unidentified HIFα interactors and, thus, control HIF target gene expression without directly regulating HIFα.

In cancer cell models, mitochondrial dysfunction promotes cell proliferation, increased tumourigenicity, invasiveness, and the epithelial-to-mesenchymal transition via retrograde signaling (7, 58). In these models, inhibition of retrograde signaling prevents these tumourigenic phenotypes. Neuronal mitochondrial dysfunction in our model causes a cellular response, resulting in a severe deficit in neuronal function. This response may have evolved to protect neurons, through decreased translation and increased glycolysis, from the short-term loss of mitochondrial function. Over longer periods, however, this response may be counterproductive because it results in decreased neuronal activity and locomotor function. Inhibition of neuronal mitochondrial retrograde signaling, through knockdown of Sima, dramatically improves neuronal function. Thus, mitochondrial retrograde signaling contributes to neuronal pathology and can be modified to improve the functional state of the neuron. Importantly, this intervention works without altering the primary mitochondrial defect. Knockdown of Sima not only abrogates the acute defects in neuronal function, but also suppresses the reduced lifespan caused by neuronal mitochondrial damage. The benefits of reduced Sima expression therefore extend throughout life.

In addition to TFAM overexpression, we also show that Sima knockdown in neurons rescues a *Drosophila* model of the mitochondrial disease Leigh syndrome. However, Sima knockdown does not rescue the lethality caused by a temperature-sensitive mutation in coxI. Mitochondrial diseases are complex, and mutations in different COX assembly factors cause varying levels of COX deficiency in different tissues (27). The increasing number of *Drosophila* models of mitochondrial dysfunction will help to unravel the mechanisms underlying the varied pathology of

mitochondrial diseases. Ubiquitous knockdown of Sima also partially restores the climbing ability of *parkin* mutant flies. The ability of reduced Sima expression to rescue both mitochondrial dysfunction and Parkinson's disease models reinforces the link between mitochondrial deficiency and Parkinson's and suggests that retrograde signaling may be a therapeutic target in Parkinson's disease. HIF1α inhibitors are in clinical trials for lymphoma and so, if our findings can be replicated in mammalian models, HIF1α inhibitors may be candidates for repurposing to treat mitochondrial diseases and neurodegenerative diseases associated with mitochondrial dysfunction, such as Parkinson's disease.

Materials and Methods

Fly Strains, Genetic Crosses, and Growth Conditions. Fly stocks were *UAS-mitoXhoI* (9), *Ilp3-lacZ* (a gift from Rita Sousa-Nunes, King's College London, London), *UAS-mito-roGFP2-Grx1* (16), *UAS-Surf1*$^{23.4}$ RNAi (31), *mt:CoI*^{T3001} (28), *park*^{25} (32). The following fly stocks were from the Bloomington Stock Centre: *w*^{1118}, *Da-Gal4*, *nSyb-Gal4*, *UAS-mitoGFP*, *OK371-Gal4*, *D42-Gal4*, *UAS-CD8GFP*, *tub-Gal80*^{ts}, *tub-Gal4*, *Thor-lacZ* (*Thor*^{K13517}), *UAS-sima*, and *sima* RNAi (HMS00832 and HMS00833). *ATPsynCF6* RNAi (107826) was from the Vienna *Drosophila* Resource Centre.

Flies were maintained on standard yeast, glucose, cornmeal, and agar food at 25 °C in a 12-h light/dark cycle unless stated otherwise. For imaging of larval motor neuron cell bodies, axons, and NMJs, embryos were laid over a 24-h period at 25 °C, incubated for a further 24 h at 25 °C, then incubated at 29 °C for 3 d before analysis. For *tub-Gal80*^{ts}*; tub-Gal4* experiments, embryos were laid for 3 d at 18 °C, then incubated for 5 d at 18 °C, followed by 3 d at 29 °C before dissection at late third larval instar stage.

Immunofluorescence and Imaging. For imaging of the larval NMJ, late third instar larvae were cut open along the dorsal midline, fixed, and stained as described in *SI Appendix, SI Materials and Methods*.

For measurement of glutathione redox potential, the dissection protocol was adapted from Albrecht et al. (16) as described in *SI Appendix, SI Materials and Methods*.

For direct imaging of the larval CNS, dissected third instar CNS tissue was fixed for 30 min in 4% (vol/vol) formaldehyde/PBS, then washed three times for 10 min in PBST and mounted in Vectashield (Vectalabs). For imaging of motor neuron cell bodies, equivalent groups of cell bodies toward the posterior of the VNC were imaged. Proximal axonal mitochondria were imaged in equivalent segmental nerves as they exited the VNC. Distal axonal mitochondria were imaged in axons of hemisegment A3, muscle 4, immediately before the NMJ. Immunostaining, TMRM, and Mitotracker Green staining of larval tissue was performed as described in *SI Appendix, SI Materials and Methods*. All imaging was performed on a Zeiss LSM 710 confocal microscope.

Transmission Electron Microscopy. Transmission electron microscopy (TEM) was performed as in Li et al. (59).

Cloning of TFAM. *UAS-TFAM* was generated by PCR amplification from clone LD40493 (DGRC) using primers Tfam.EcoRI.Fw and Tfam.XbaI.Rv (*SI Appendix*, Table S5). The PCR product was then cloned into EcoRI and XbaI sites in pUAST (DGRC). The TFAM cDNA was confirmed by Sanger sequencing. Transgenic flies were generated by BestGene. Stocks containing *UAS-TFAM* insertions on the second (*UAS-TFAM3M*) and third (*UAS-TFAM10M*) chromosome were used. *UAS-TFAM3M* is expressed more strongly than *UAS-TFAM10M*.

Quantitative PCR of mtDNA. Genomic DNA was prepared from late third instar larvae by using a standard potassium acetate/phenol-chloroform method. Real-time quantitative PCR (qPCR) was performed by using 25 ng of genomic DNA with the SensiMix SYBR No-ROX kit (Bioline), using a Corbett Rotor-Gene RG-3000 machine and primers for the mitochondrial gene *coxI* and the nuclear gene *Gapdh1* (*SI Appendix*, Table S5). qPCRs were carried out for 40 cycles (95 °C for 10 s, 60 °C for 15 s, and 72 °C for 20 s). CT values for *coxI* and *Gapdh1* were then used to calculate the ΔCT between these two genes for each sample. This value was used as the relative mtDNA level. Standard curves for *coxI* and *Gapdh1*, using a series of eight (threefold) dilutions of genomic DNA, were run in all experiments to determine the efficiency of the reaction and were only used when the efficiency was >95%. For qPCR across the mtDNA XhoI site primers, XhoI-F/R were used together with *Gapdh1* primers (*SI Appendix*, Table S5).

Quantitative Reverse Transcription-PCR (qRT-PCR). Three third instar larvae were homogenized in 0.1 mL of TRIzol Reagent (Life Technologies), RNA was extracted according to manufacturer's instructions and diluted to 150 ng/μL. RNA was treated with DNase I (Sigma-Aldrich) following manufacturer's directions. cDNA was synthesized by using random primers with the First Strand cDNA synthesis kit (Fermentas). PCR was performed with qPCRBIO Sygreen Mix Lo-ROX (PCRBiosystems) by using 30 ng/μL cDNA on a Roche Lightcycler 480 Instrument II. The program was 95 °C for 10 min, then 35 cycles of 95 °C for 10 s, 60 °C for 15 s, 72 °C for 20 s, and finally increasing from 72 °C to 95 °C. All samples were measured in triplicate and compared with levels of the housekeeping gene *ribosomal protein L4* (*Rpl4*). CT values for target gene and *RpL4* were used to calculate the ΔCT between these two genes. Standard curves using a series of eight (threefold) dilutions of cDNA were run to determine the efficiency of the reaction was >95%. Primers used are shown in *SI Appendix*, Table S5.

Western Blot Analysis. Twenty-five larvae per genotype were homogenized in 150 μL of 1× SDS/PAGE loading buffer and analyzed by SDS/PAGE. Primary antibodies were rabbit anti-*Drosophila* TFAM (Abcam; ab47548, 1:500), mouse anti-ATP5A (Abcam; ab14748, 1:5,000), mouse anti-MTCO1 (Abcam; ab14705, 1:1,000), and rabbit anti-Actin (Cell Signaling; 1:4,000). Normalized expression level was calculated by determining the band intensity relative to Actin.

Behavioral and Lifespan Analysis. For viability assays, 50 first instar larvae per genotype were transferred to a single vial and the number of eclosed adult flies counted from each vial. Flies from six vials were counted for each genotype.

Adult climbing assays were performed on 2- to 3-d-old male flies. Adult flies were anesthetized by using CO_2 and male flies separated into a new vial and left for 24 h at 25 °C to recover. Using a mouth aspirator, a single fly was transferred to a 5-mL pipette (Falcon), with the tip removed. The pipette was then inverted and tapped onto the bench so that the fly fell to the bottom. The distance climbed by each fly was measured after 10 s of continuous climbing (runs in which flies paused during the climb were ignored). Each fly was tested three times, and between 10 and 14 flies were tested for each genotype. Climbing assays were performed between 8:00 a.m. (1 h after illumination) and 10:00 a.m. For climbing assays using *UAS-TFAM10M*, flies were grown at 29 °C.

For lifespan assays, flies were separated in vials according to genotype (10 flies per vial) and kept at 25 °C. Flies were flipped into fresh vials twice a week, and dead flies were counted three times a week.

Microarray Experiments and Analysis. The CNS from 15 wandering third instar control (*nSyb-Gal4/w*^{1118}), TFAM overexpressing (*nSyb-Gal4/UAS-TFAM*), or *ATPsynCF6* RNAi (*nSyb-Gal4/UAS-ATPsynCF6* RNAi) larvae were dissected in PBS, placed into PBS on ice, then transferred into 100 μL of lysis buffer from the Absolutely RNA Microprep kit (Stratagene) and vortexed for 5 s. Total RNA was then prepared according to the manufacturer's instructions. For each genotype, RNA samples were prepared in triplicate and stored at −80 °C. cDNA was prepared from 500 ng of total RNA by using the Ambion WT Expression kit. Hybridizations were performed by using the Affymetrix Terminal Labeling kit on *Drosophila* Gene 1.0 ST Arrays (Affymetrix). Imaging of the arrays was performed by using the Affymetrix GCS3000 microarray system. The data discussed in this publication have been deposited in NCBI's Gene Expression Omnibus and are accessible through GEO Series accession no. GSE53509.

Microarray data were processed by using a Robust Multichip Average (RMA) *F* (60) algorithm and analyzed by using the Omics Explorer package v2.3 (Qlucore). A false discovery rate of 0.2% was used. GO analysis was performed by using DAVID (the database for annotation, visualization and integrated discovery) bioinformatics resources (61).

Quantification and Statistical Analysis. Bouton number and active zone number were quantified in larvae expressing *UAS-CD8-GFP* driven by *OK371-Gal4* and only type IB boutons were included. Active zone number (the number of brp puncta), mitochondrial number, and volume were quantified by using the Measurement tool in Volocity (PerkinElmer). Ten to 12 NMJs (from 5 to 6 larvae) were quantified for each genotype for bouton number, mitochondrial number and mitochondrial volume, and 18–20 NMJs (from 9 to 10 larvae) for active zone number. Axonal mitochondria were quantified by determining mitochondrial number and volume in rectangles of 50 × 150 pixels (3.7 × 11 μm) for proximal axons and 50 × 100 pixels (3.7 × 7.3 μm) for distal axons. Three (proximal axons) or two (distal axons) rectangles were used in four different axons from different larvae for each genotype.

Thor-lacZ expression in motor neuron cell bodies was measured as intensity by using the point tool in ImageJ. The intensity of 20–25 cells per VNC were measured and averaged to give a single value. *Ilp3-lacZ* expression in seven median neurosecretory neurons per brain hemisphere was measured as intensity by using the point tool in ImageJ and averaged. TMRM was measured as intensity by using the point tool in ImageJ and averaged.

Statistical analysis was performed in GraphPad Prism 5. Statistical significance was determined by using an unpaired Student's *t* test for pairwise

comparisons, or one-way analysis of variance (ANOVA) with Dunnett's multiple comparison post hoc test for multiple comparisons to the control, or ANOVA with Tukey's post hoc test for comparisons between genotypes. For lifespan assays, the log-rank test was used to calculate *P* values, and the significant threshold was adjusted for multiple comparisons. Fisher's exact test was used to compare significantly regulated genes from microarray studies and for analysis of the wing inflation data.

ACKNOWLEDGMENTS. We thank Meg Stark (University of York Biology Technology Facility) and Ryan West for assistance with the TEM; Gareth Williams for advice on statistics; Pat O'Farrell, Rodolfo Costa, and Rita Sousa-Nunes for fly stocks; and Hong Xu and Alexander Whitworth for fly stocks and helpful advice. This work was funded by Wellcome Trust Grant WT089622MA, Biotechnology and Biological Sciences Research Council Grant BB/I012273/1, the National Institute for Health Research (NIHR), the Biomedical Research Centre at King's College London (KCL), and KCL.

1. Coskun P, et al. (2012) A mitochondrial etiology of Alzheimer and Parkinson disease. *Biochim Biophys Acta* 1820(5):553–564.
2. Schaefer AM, et al. (2008) Prevalence of mitochondrial DNA disease in adults. *Ann Neurol* 63(1):35–39.
3. Ylikallio E, Suomalainen A (2012) Mechanisms of mitochondrial diseases. *Ann Med* 44(1):41–59.
4. Scheibye-Knudsen M, Fang EF, Croteau DL, Wilson DM, 3rd, Bohr VA (2015) Protecting the mitochondrial powerhouse. *Trends Cell Biol* 25(3):158–170.
5. Butow RA, Avadhani NG (2004) Mitochondrial signaling: The retrograde response. *Mol Cell* 14(1):1–15.
6. Cagin U, Enriquez JA (2015) The complex crosstalk between mitochondria and the nucleus: What goes in between? *Int J Biochem Cell Biol* 63:10–15.
7. Guha M, Avadhani NG (2013) Mitochondrial retrograde signaling at the crossroads of tumor bioenergetics, genetics and epigenetics. *Mitochondrion* 13(6):577–591.
8. Correia SC, et al. (2012) Mitochondrial importance in Alzheimer's, Huntington's and Parkinson's diseases. *Adv Exp Med Biol* 724:205–221.
9. Xu H, DeLuca SZ, O'Farrell PH (2008) Manipulating the metazoan mitochondrial genome with targeted restriction enzymes. *Science* 321(5888):575–577.
10. Ylikallio E, Tyynismaa H, Tsutsui H, Ide T, Suomalainen A (2010) High mitochondrial DNA copy number has detrimental effects in mice. *Hum Mol Genet* 19(13):2695–2705.
11. Falkenberg M, et al. (2002) Mitochondrial transcription factors B1 and B2 activate transcription of human mtDNA. *Nat Genet* 31(3):289–294.
12. Maniura-Weber K, Goffart S, Garstka HL, Montoya J, Wiesner RJ (2004) Transient overexpression of mitochondrial transcription factor A (TFAM) is sufficient to stimulate mitochondrial DNA transcription, but not sufficient to increase mtDNA copy number in cultured cells. *Nucleic Acids Res* 32(20):6015–6027.
13. Pohjoismäki JL, et al. (2006) Alterations to the expression level of mitochondrial transcription factor A, TFAM, modify the mode of mitochondrial DNA replication in cultured human cells. *Nucleic Acids Res* 34(20):5815–5828.
14. Luan H, et al. (2006) Functional dissection of a neuronal network required for cuticle tanning and wing expansion in Drosophila. *J Neurosci* 26(2):573–584.
15. Vanden Broeck L, et al. (2013) TDP-43 loss-of-function causes neuronal loss due to defective steroid receptor-mediated gene program switching in Drosophila. *Cell Reports* 3(1):160–172.
16. Albrecht SC, Barata AG, Grosshans J, Teleman AA, Dick TP (2011) In vivo mapping of hydrogen peroxide and oxidized glutathione reveals chemical and regional specificity of redox homeostasis. *Cell Metab* 14(6):819–829.
17. Carbajo RJ, et al. (2005) Structure of the F1-binding domain of the stator of bovine F1Fo-ATPase and how it binds an alpha-subunit. *J Mol Biol* 351(4):824–838.
18. Zoncu R, Efeyan A, Sabatini DM (2011) mTOR: From growth signal integration to cancer, diabetes and ageing. *Nat Rev Mol Cell Biol* 12(1):21–35.
19. Fernández-Ayala DJ, Chen S, Kemppainen E, O'Dell KM, Jacobs HT (2010) Gene expression in a Drosophila model of mitochondrial disease. *PLoS One* 5(1):e8549.
20. Freije WA, Mandal S, Banerjee U (2012) Expression profiling of attenuated mitochondrial function identifies retrograde signals in Drosophila. *G3 (Bethesda)* 2(8):843–851.
21. Tufi R, et al. (2014) Enhancing nucleotide metabolism protects against mitochondrial dysfunction and neurodegeneration in a PINK1 model of Parkinson's disease. *Nat Cell Biol* 16(2):157–166.
22. Majmundar AJ, Wong WJ, Simon MC (2010) Hypoxia-inducible factors and the response to hypoxic stress. *Mol Cell* 40(2):294–309.
23. Ebert BL, Firth JD, Ratcliffe PJ (1995) Hypoxia and mitochondrial inhibitors regulate expression of glucose transporter-1 via distinct Cis-acting sequences. *J Biol Chem* 270(49):29083–29089.
24. Firth JD, Ebert BL, Ratcliffe PJ (1995) Hypoxic regulation of lactate dehydrogenase A. Interaction between hypoxia-inducible factor 1 and cAMP response elements. *J Biol Chem* 270(36):21021–21027.
25. Lavista-Llanos S, et al. (2002) Control of the hypoxic response in Drosophila melanogaster by the basic helix-loop-helix PAS protein similar. *Mol Cell Biol* 22(19):6842–6853.
26. Li Y, et al. (2013) HIF- and non-HIF-regulated hypoxic responses require the estrogen-related receptor in Drosophila melanogaster. *PLoS Genet* 9(1):e1003230.
27. Shoubridge EA (2001) Cytochrome c oxidase deficiency. *Am J Med Genet* 106(1):46–52.
28. Chen Z, et al. (2015) Genetic mosaic analysis of a deleterious mitochondrial DNA mutation in Drosophila reveals novel aspects of mitochondrial regulation and function. *Mol Biol Cell* 26(4):674–684.
29. Tiranti V, et al. (1998) Mutations of SURF-1 in Leigh disease associated with cytochrome c oxidase deficiency. *Am J Hum Genet* 63(6):1609–1621.
30. Zhu Z, et al. (1998) SURF1, encoding a factor involved in the biogenesis of cytochrome c oxidase, is mutated in Leigh syndrome. *Nat Genet* 20(4):337–343.
31. Zordan MA, et al. (2006) Post-transcriptional silencing and functional characterization of the Drosophila melanogaster homolog of human Surf1. *Genetics* 172(1):229–241.
32. Greene JC, et al. (2003) Mitochondrial pathology and apoptotic muscle degeneration in Drosophila parkin mutants. *Proc Natl Acad Sci USA* 100(7):4078–4083.
33. Iyengar B, Luo N, Farr CL, Kaguni LS, Campos AR (2002) The accessory subunit of DNA polymerase gamma is essential for mitochondrial DNA maintenance and development in Drosophila melanogaster. *Proc Natl Acad Sci USA* 99(7):4483–4488.
34. Iyengar B, Roote J, Campos AR (1999) The tamas gene, identified as a mutation that disrupts larval behavior in Drosophila melanogaster, codes for the mitochondrial DNA polymerase catalytic subunit (DNApol-gamma125). *Genetics* 153(4):1809–1824.
35. Ekstrand MI, et al. (2004) Mitochondrial transcription factor A regulates mtDNA copy number in mammals. *Hum Mol Genet* 13(9):935–944.
36. Wang X, et al. (2011) PINK1 and Parkin target Miro for phosphorylation and degradation to arrest mitochondrial motility. *Cell* 147(4):893–906.
37. Ashrafi G, Schlehe JS, LaVoie MJ, Schwarz TL (2014) Mitophagy of damaged mitochondria occurs locally in distal neuronal axons and requires PINK1 and Parkin. *J Cell Biol* 206(5):655–670.
38. Ekstrand MI, et al. (2007) Progressive parkinsonism in mice with respiratory-chain-deficient dopamine neurons. *Proc Natl Acad Sci USA* 104(4):1325–1330.
39. Pickrell AM, Pinto M, Hida A, Moraes CT (2011) Striatal dysfunctions associated with mitochondrial DNA damage in dopaminergic neurons in a mouse model of Parkinson's disease. *J Neurosci* 31(48):17649–17658.
40. Galter D, et al. (2010) MitoPark mice mirror the slow progression of key symptoms and L-DOPA response in Parkinson's disease. *Genes Brain Behav* 9(2):173–181.
41. Sterky FH, Lee S, Wibom R, Olson L, Larsson NG (2011) Impaired mitochondrial transport and Parkin-independent degeneration of respiratory chain-deficient dopamine neurons in vivo. *Proc Natl Acad Sci USA* 108(31):12937–12942.
42. Verstreken P, et al. (2005) Synaptic mitochondria are critical for mobilization of reserve pool vesicles at Drosophila neuromuscular junctions. *Neuron* 47(3):365–378.
43. Zhao XL, et al. (2010) Expression of beta-amyloid induced age-dependent presynaptic and axonal changes in Drosophila. *J Neurosci* 30(4):1512–1522.
44. Baloyannis SJ, Costa V, Michmizos D (2004) Mitochondrial alterations in Alzheimer's disease. *Am J Alzheimers Dis Other Demen* 19(2):89–93.
45. Scheff SW, Price DA (2006) Alzheimer's disease-related alterations in synaptic density: Neocortex and hippocampus. *J Alzheimers Dis* 9(3, Suppl):101–115.
46. McCammon MT, Epstein CB, Przybyla-Zawislak B, McAlister-Henn L, Butow RA (2003) Global transcription analysis of Krebs tricarboxylic acid cycle mutants reveals an alternating pattern of gene expression and effects on hypoxic and oxidative genes. *Mol Biol Cell* 14(3):958–972.
47. Jahangir Tafrechi RS, et al. (2005) Distinct nuclear gene expression profiles in cells with mtDNA depletion and homoplasmic A3243G mutation. *Mutat Res* 578(1-2):43–52.
48. Picard M, et al. (2014) Progressive increase in mtDNA 3243A>G heteroplasmy causes abrupt transcriptional reprogramming. *Proc Natl Acad Sci USA* 111(38):E4033–E4042.
49. Guha M, Srinivasan S, Biswas G, Avadhani NG (2007) Activation of a novel calcineurin-mediated insulin-like growth factor-1 receptor pathway, altered metabolism, and tumor cell invasion in cells subjected to mitochondrial respiratory stress. *J Biol Chem* 282(19):14536–14546.
50. Amuthan G, et al. (2001) Mitochondria-to-nucleus stress signaling induces phenotypic changes, tumor progression and cell invasion. *EMBO J* 20(8):1910–1920.
51. Biswas G, Anandatheerthavarada HK, Avadhani NG (2005) Mechanism of mitochondrial stress-induced resistance to apoptosis in mitochondrial DNA-depleted C2C12 myocytes. *Cell Death Differ* 12(3):266–278.
52. Chandel NS, et al. (2000) Reactive oxygen species generated at mitochondrial complex III stabilize hypoxia-inducible factor-1alpha during hypoxia: A mechanism of O2 sensing. *J Biol Chem* 275(33):25130–25138.
53. Chua YL, et al. (2010) Stabilization of hypoxia-inducible factor-1alpha protein in hypoxia occurs independently of mitochondrial reactive oxygen species production. *J Biol Chem* 285(41):31277–31284.
54. Raimundo N, et al. (2012) Mitochondrial stress engages E2F1 apoptotic signaling to cause deafness. *Cell* 148(4):716–726.
55. Owusu-Ansah E, Yavari A, Mandal S, Banerjee U (2008) Distinct mitochondrial retrograde signals control the G1-S cell cycle checkpoint. *Nat Genet* 40(3):356–361.
56. Ao A, Wang H, Kamarajugadda S, Lu J (2008) Involvement of estrogen-related receptors in transcriptional response to hypoxia and growth of solid tumors. *Proc Natl Acad Sci USA* 105(22):7821–7826.
57. Sánchez-Elsner T, et al. (2001) Synergistic cooperation between hypoxia and transforming growth factor-beta pathways on human vascular endothelial growth factor gene expression. *J Biol Chem* 276(42):38527–38535.
58. Guha M, et al. (2014) Mitochondrial retrograde signaling induces epithelial-mesenchymal transition and generates breast cancer stem cells. *Oncogene* 33(45):5238–5250.
59. Li X, et al. (2010) Bicaudal-D binds clathrin heavy chain to promote its transport and augments synaptic vesicle recycling. *EMBO J* 29(5):992–1006.
60. Irizarry RA, et al. (2003) Summaries of Affymetrix GeneChip probe level data. *Nucleic Acids Res* 31(4):e15.
61. Huang W, Sherman BT, Lempicki RA (2009) Systematic and integrative analysis of large gene lists using DAVID bioinformatics resources. *Nat Protoc* 4(1):44–57.